Slip slope change detection based on active drive force excitation

Journal Title
XX(X):1–10

DOI: 10.1177/ToBeAssigned
www.sagepub.com/
SAGE

Andreas Fichtinger[1], Johannes Edelmann[1], Manfred Plöchl[1], Manuel Höll[2], Michael Unterreiner[3]

Abstract

Identification of the available friction potential is crucial for road safety but difficult, in particular at normal driving. This paper aims to contribute by presenting an effect-based method for slip slope change detection related to friction potential changes at all wheel-drive vehicles applying active drive force excitation. The proposed estimation approach relies above all on the wheel speeds and the axle/wheel drive forces of the front and rear axle. Different types of periodic active drive force excitation that are superimposed to the drive force requested by the driver while maintaining the desired level of speed or acceleration are investigated w.r.t. the availability of the estimates and overall effectiveness of the estimator. Vehicle tests are performed to evaluate theoretical results and the (co-)driver's perception of the active drive force excitation. Results from both the simulation study and vehicle tests show that the proposed method allows to reliably estimate slip slope changes at all-wheel drive vehicles in driving conditions with low levels of drive force excitation.

Keywords

slip stiffness estimation, tire-road friction estimation, differential slip, active drive force excitation

Introduction

Knowledge of the available tire–road friction potential is most relevant for the human and robot driver to adjust vehicle speed accordingly. Moreover, advanced driver assist systems may adopt parameters accordingly to guarantee comfort and safety. In literature, several approaches to estimate road surface conditions and related tire–road friction potential are proposed. In general, respective methods may be categorized as cause-based and effect-based. Cause-based methods utilize sensors to gain information on the ambient conditions to extrapolate the friction potential, whereas effect-based methods rely on observed reactions of the vehicle and its subsystems, resulting from (changing) tire–road contact conditions.[1] While sensors applied at cause-based methods may provide some preview, effect-based methods allow to estimate the friction potential from the actual tire and road pairing. Estimated tire–road friction potential may be augmented on-board, e.g. from cloud-based services, or may be shared with other vehicles or with the cloud.[2]

Effect-based methods require a sufficiently high level and variation of excitation to allow to estimate indicators of the actual tire–road friction potential. Hence, respective utilization of the available friction potential – where the tire is operated in its nonlinear regime – is needed e.g. from brake/drive or lateral force excitation.[1,3–5] However, sufficient friction potential utilization is rarely requested by the driver at normal driving at high-friction road surface conditions. Moreover, at driving smoothly on country roads or motorways, the variation of the excitation level is small. Thus, availability of respective estimates is very limited.

To overcome the lack of excitation, e.g. active brake/drive force excitation of the tires is proposed.[6,7] Lajewski et al.[6] suggested to brake a single wheel of an automobile until it reaches the friction limit, where an expert driver has to keep the vehicle on track. This approach is considered for friction potential classification of public roads, similar to friction test trailers used by road authorities.[8] In contrast, Albinsson et al.[7] introduced a method based on active drive force excitation, which is considered to be applicable in regular driving. Rather large longitudinal driving forces are generated at one axle by applying brake forces on the opposite axle, while maintaining the vehicle motion desired by the driver at low levels of acceleration, e.g. at driving on a highway.

Appropriate optimal drive force excitation strategies are studied by Albinsson et al.[5], where the focus has been put to the impact on friction potential estimation errors, depending on the tire models applied in respective estimation algorithms. It was concluded that about 60 % utilization of the actual tire–road friction potential is required for reliable estimation of the friction potential.

From field measurements, different tire slip slopes at different road surface conditions have been identified by Dieckmann[9] and others[10–16]. Similar findings are presented in Figure 1 for dry asphalt, asphalt and ice covered with snow, and polished ice. Inter-layer effects between tire

[1]TU Wien, Institute of Mechanics and Mechatronics, Technical Dynamics and Vehicle System Dynamics, Austria
[2]Dr. Ing. h.c. F. Porsche AG, Germany
[3]CARIAD SE, Germany

Corresponding author:
Johannes Edelmann, TU Wien, Institute of Mechanics and Mechatronics, Technical Dynamics and Vehicle System Dynamics, Austria
Email: johannes.edelmann@tuwien.ac.at

contact patch and road surface have been identified to explain the changes of measured slip slope.[1,12] Since the level of drive/brake force excitation required to measure these effects are rather low, higher availability of respective estimates might be expected. However, the measured slip slope (change) is not directly related to the maximum friction potential.[11,14] Further, slip slope is sensitive to other parameters than road surface condition, e.g. inflation pressure and temperature.[13] Therefore, knowledge of the actual slip slope only does not allow for reliable tire–road friction potential estimation. Nevertheless, a sudden change of the slip slope of the tire might be an indicator for changed road surface conditions, and a corresponding drop indicates a drop of the maximum friction potential.

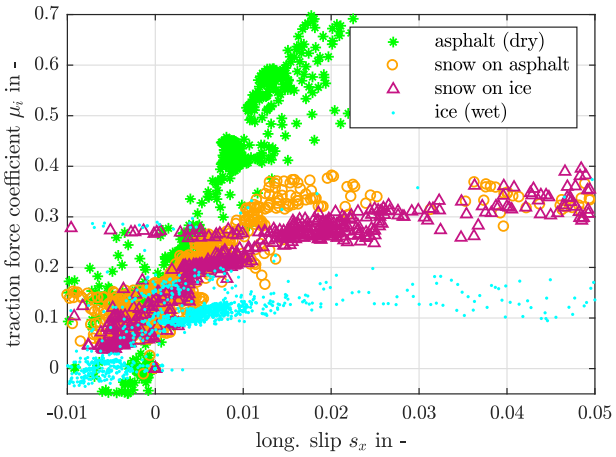

Figure 1. Traction coefficient – slip curves from field measurements of a winter tire (295/30R20) on dry asphalt, asphalt and ice covered with snow, and polished ice.

An approach to estimate the slip slope in real-time is presented by Gustafsson[10,11], utilizing a linear tire model and a Kalman filter, where longitudinal velocity for slip calculation is derived from the angular velocity of the non-driven wheels. While braking and for all-wheel drive vehicles, longitudinal velocity has to be provided from other sources, like GPS-measurements or state estimators based on wheel speeds and acceleration.[17,18] However, since slip quantities are rather small, slip calculation – and respective slip slope estimation – is sensitive to errors in longitudinal velocity and tire effective rolling radius (estimation), and with respect to measurement noise and time delays resulting from measurement, filtering and vehicle BUS communication.

To avoid the need for accurate knowledge of the actual tire slip (and thus related quantities), a method to estimate the tire slip slope based on a measured 'average' slip of two tires is presented by Forssell et al.[19] The measured slip quantity is calculated form the difference of the wheel speed of one tire, e.g. at the front axle, with respect to a second tire, typically from the opposite axle. Slip slope parameters for both tires can either be estimated independently or, assuming equal tire slip stiffness on both wheels, together as one parameter. The method is applicable as long as the drive force is not equal for both wheels and signal to noise ratio of the tire slip is sufficient.[11]

A recent review on tire–road friction potential estimation in particular at low levels of excitation is given by Acosta et al.[20] It is concluded that current methods either focus on high longitudinal or lateral tire forces for direct estimation of the tire–road friction coefficient, or on the linear longitudinal tire characteristic which needs accurate slip measures. With focus on normal driving on country roads and highways and in particular at all-wheel drive vehicles, high levels of tire force utilisation occurs rarely and longitudinal slip may not be available in a sufficient quality. Moreover, low variation of tire slip/forces is challenging from the numerical estimator point of view.[21] Therefore, availability of valid estimates is limited and slip slope changes may be detected late.

In this paper, an approach to estimate longitudinal slip slope changes as an indicator for maximum tire-road friction potential changes is presented. This approach makes use of active drive(/recuperation) force distribution at all-wheel drive (electric) vehicles to allow for high availability of estimates and relies on known wheel speeds and drive/recuperation forces only. The estimator is based on the differential slip between the front and rear driven tires, similar to Forssell et al.[19], taking into account that tires may have different tire properties, in particular slip stiffness, e.g. due to nominal load, mixed tires or tire wear. The focus is put on rather low levels of active drive forces excitations to allow for effective slip slope change estimation in normal driving conditions and to avoid potential vehicle stability issues on low friction road surfaces.

The estimation method is presented in the subsequent section, and the impact of different drive force distributions and levels of excitation is discussed. The effectiveness of constant and active drive force distribution strategies considering the level of excitation will be studied by means of numerical simulation. Finally, results from test drives with a prototype vehicle with active drive force distributions are presented to validate the theoretical findings.

Estimation Method

The derivation of the estimator will be presented next, and the impact of the drive force distribution at all-wheel drive (electric) vehicles on the utilization of the effective slip–tire force curve will be discussed.

System model and Kalman filter

The presented method aims to enable slip slope change detection for all-wheel drive vehicles in normal driving situations with constant velocities or low levels of longitudinal acceleration. To map the tire characteristics at these rather low levels of longitudinal force excitation and related small, quasi-steady state wheel load transfer, a linear approach is assumed,

$$\mu_i = \overline{C}_{s_x,i}\, s_{x,i} - \overline{C}_{s_x,i}\, \delta_i \qquad i = F, R \tag{1}$$

with the mean values of the traction coefficient $\mu_i = F_{x,i}/F_{z,i}$, slip $s_{x,i}$, normalized slip slope $\overline{C}_{s_x,i} = C_{s_x,i}/F_{z,i}$, and slip offset δ_i of the front and rear axle tires. To avoid the need for knowledge of the longitudinal velocity of the vehicle for slip slope estimation, similar to Gustafsson[10], the vehicle's velocity is eliminated

from the longitudinal slip

$$s_{x,i} = \frac{\omega_i\, r_{e,i} \;-\; v_x}{\omega_i\, r_{e,i}} \qquad i = F, R \tag{2}$$

(mean wheel speed ω_i and effective rolling radius $r_{e,i}$ of the front (F) and rear (R) axle, and longitudinal velocity v_x of the vehicle), resulting in two redundant equations:

$$s_{x,j} \;=\; \underbrace{\frac{r_{e,j}\,\omega_j - r_{e,k}\,\omega_k}{r_{e,j}\,\omega_j}}_{s_{x,\Delta,j}} + \frac{r_{e,k}\,\omega_k}{r_{e,j}\,\omega_j}\, s_{x,k} \qquad j = F,\, k = R \text{ and } j = R,\, k = F \tag{3}$$

$s_{x,\Delta,j}$ is a measure for relative speed difference between front and rear axle speeds based on tire radii and measured wheel speeds only, and is further referred to as differential slip. After rearrangement of equation (3), this relation becomes more obvious, since $s_{x,\Delta,j}$ can be written as a scaled difference between the slip measures of the front and rear axle,

$$s_{x,\Delta,j} = s_{x,j} - \frac{r_{e,k}\,\omega_k}{r_{e,j}\,\omega_j}\, s_{x,k} \qquad j = F,\, k = R \text{ or } j = R,\, k = F \tag{4}$$

The nominal value of the slip stiffness $C_{s_x,i}$ at different axles may differ because of different tire type, size, wear, inflation pressure, nominal loads etc. Assuming that these changes progress slowly, while changes of the road surface and therefore of the slip slope appear suddenly and at both axles of the vehicle, the following slip stiffness ratio λ is introduced,

$$\lambda = \frac{C_{s_x,R}/F_{z,R}}{C_{s_x,F}/F_{z,F}} = \frac{\overline{C}_{s_x,R}}{\overline{C}_{s_x,F}} \quad \Rightarrow \quad \overline{C}_{s_x,R} = \lambda\, \overline{C}_{s_x,F} \tag{5}$$

that allows for estimation of the fast changing normalized slip slope to indicate friction potential changes and the slowly varying slip stiffness ratio with different dynamics.

Substituting (3) into (1) and making use of (5) yields the (redundant) equations for the estimation approach, formulated for the front and rear axle,

$$s_{x,\Delta,F} = \underbrace{\left(\mu_F \;-\; \frac{1}{\lambda}\,\frac{r_{e,R}\,\omega_R}{r_{e,F}\,\omega_F}\,\mu_R\right)}_{\mu_{\Delta,F}} \frac{1}{\overline{C}_{s_x,F}} + \underbrace{\left(\delta_F \;-\; \frac{r_{e,R}\,\omega_R}{r_{e,F}\,\omega_F}\,\delta_R\right)}_{\overline{\delta}_F} \tag{6a}$$

$$s_{x,\Delta,R} = \underbrace{\left(\mu_R \;-\; \lambda\,\frac{r_{e,F}\,\omega_F}{r_{e,R}\,\omega_R}\,\mu_F\right)}_{\mu_{\Delta,R}} \frac{1}{\overline{C}_{s_x,R}} + \underbrace{\left(\delta_R \;-\; \frac{r_{e,F}\,\omega_F}{r_{e,R}\,\omega_R}\,\delta_F\right)}_{\overline{\delta}_R} \tag{6b}$$

Similar to the differential slip $s_{x,\Delta,i}$, the first term composed by the scaled difference of traction coefficients is denoted the differential traction coefficient $\mu_{\Delta,i}$. The scaled slip offsets of the front and rear axle are merged to a generalized offset parameter $\overline{\delta}_i$. The parameters to be estimated are the normalized slip slope $\overline{C}_{s_x,i}$, the slip stiffness ratio λ and the generalized slip offset parameter $\overline{\delta}_i$. The ratio of the effective roll radii of the front and rear tires in (6) can be estimated e.g. at coasting, no absolute radii are needed.

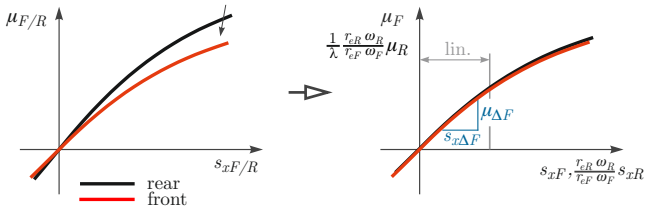

Figure 2. Scaling of tire(/axle) characteristics for determination of differential slip $s_{x,\Delta,F}$ and differential traction coefficient $\mu_{\Delta,F}$ (offset $\overline{\delta}_F$ not considered)

Influence of drive force distribution

Considering (6), it becomes obvious that for certain combinations of utilized traction coefficients μ_i the differential traction coefficient $\mu_{\Delta,i}$ may become zero, although the traction force at the individual axles is unequal to zero. Thus, drive force distribution may have a significant impact on the quality and availability of slip slope estimates. To give a brief illustrative explanation and to identify beneficial types of excitation at utilizing the proposed approach, the formulation w.r.t. the front axle, (6a), is discussed. Figure 2 shows a schematic drawing of the traction coefficient plotted over the longitudinal slip of both the front and rear axle on the left (neglecting the slip offset δ_i). Elimination of the vehicle's velocity from the slip definition (3) and introducing the slip stiffness ratio λ basically scales the original traction force–slip curve of one axle in order to coincide with the traction force–slip curve of the opposite axle (in the 'linear' regime), Figure 2(right). The slip scaling quantity can be directly read from equation (4), and the scaling quantity of the traction coefficient from the differential traction coefficient $\mu_{\Delta,F}$ in equation (6a). Thus, knowledge on the actual traction coefficients μ_i and on the differential slip $s_{x,\Delta,j}$ between the tires at the front and rear axle allows to estimate the normalized slip slope $\overline{C}_{s_x,j}$ of the tires at the axle, which has been considered for the formulation of (6) (which is the front axle F in Figure 2).

To gain some basic insight into the sensitivity of (6) on the drive force distribution and corresponding differential traction coefficient $\mu_{\Delta,i}$, the surface of differential traction coefficients $\mu_{\Delta,F}$ over front axle slip $s_{x,F}$ and front differential slip $s_{x,\Delta,F}$ is plotted in Figure 3(a), applying the pure longitudinal slip tire brush model[22] for mixed tires front/rear, assuming a maximum friction potential $\mu_{\max} = 1$ and a wheel load ratio $F_{z,F}/F_{z,R} = 40/60$. In addition, the projection of this surface to the $s_{x,\Delta,F}$-$\mu_{\Delta,F}$-plane is depicted in Figure 3(b). Solid lines of varied traction force utilization at constant drive force distributions are plotted ranging from front wheel drive (drive force distribution $\nu = 0$) to rear wheel drive ($\nu = 1$).

Considering the front wheel drive case it becomes obvious that for a given differential traction coefficient $\mu_{\Delta,F}$ the longitudinal slip $s_{x,F}$ at the front axle and the front

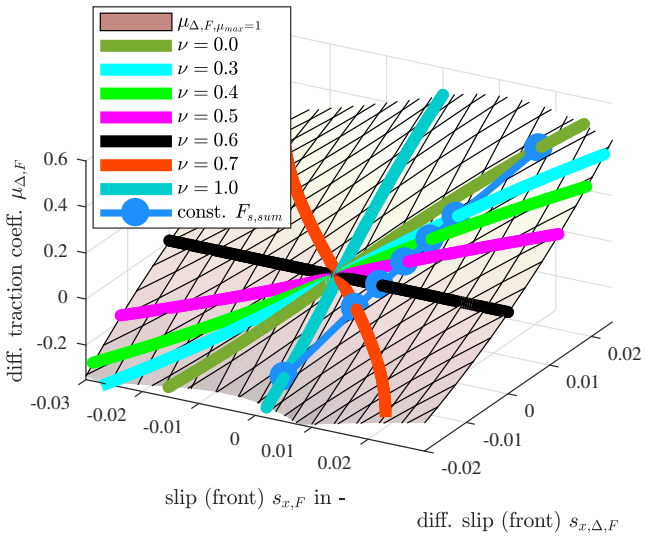

(a) Differential traction coefficient $\mu_{\Delta,F}$ over front axle slip $s_{x,F}$ and front differential slip $s_{x,\Delta,F}$.

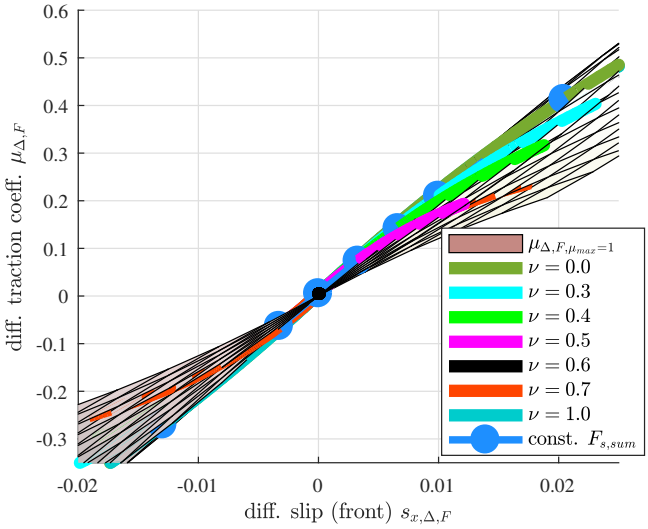

(b) Projection of (a) to the $s_{x,\Delta,F}$-$\mu_{\Delta,F}$-plane.

Figure 3. Differential traction coefficient $\mu_{\Delta,F}$, trajectories of constant drive force distributions, and trajectory of constant effective traction force $F_{x,\text{sum}}$.

differential slip $s_{x,\Delta,j}$ are equal, thus $\mu_{\Delta,F}$ corresponds to the actual traction force coefficient μ_F. When moving the traction force distribution from the front to the rear while the effective traction force of both axles $F_{x,\text{sum}}$ (and thus longitudinal acceleration of the vehicle) remains unchanged, $s_{x,F}$, $s_{x,\Delta,F}$, and $\mu_{\Delta,F}$ decrease accordingly, blue dots and lines in Figure 3. It turns out that at a particular drive force distribution, changes in the effective traction force, do not affect the resulting differential traction coefficients $\mu_{\Delta,F}$. For the front and rear tire characteristics considered in Figure 3, this is the case for drive force distributions close to $\nu = 0.6$, indicating equal traction force utilization at the front and rear axle, which may be beneficial from a safety perspective. In particular in this condition, the estimation of the normalized slip slope $\overline{C}_{s_x,j}$ of the tires is not effective.

Active excitation

To increase the availability of estimations of the normalized slip slope $\overline{C}_{s_x,i}$ and related maximum tire–road friction potential changes at very low and constant levels of drive force excitation[21], and to allow for effective estimation in conditions of unfavorable drive force distributions, an active longitudinal tire force excitation is proposed.

The nominal tire forces (and respective tire slip values) correspond to the acceleration demanded by the human/robot driver and the pre-set drive force distribution between the front and the rear axle. The active force excitation is superimposed to the nominal value of each axle, where the sum of the nominal drive forces of both axles $F_{x,\text{sum}}$ is kept constant, maintaining the current speed or acceleration demands,

$$F_{x,F} = (1-\nu)F_{x,\text{sum}} + F_{x,\text{exc}}(t)$$
$$F_{x,R} = \nu F_{x,\text{sum}} - F_{x,\text{exc}}(t)$$

with pre-set drive force distribution ν and time-dependent excitation force $F_{x,\text{exc}}$. Superimposed excitations may be transient or periodic. Transient excitation trajectories may be of interest at changing the overall drive force distribution of the vehicle e.g. based on the drive force requested by the driver/driving robot. Since we like to focus at rather small (overall) drive force levels e.g. at slightly accelerating or running at constant velocity, subsequently, reasonable periodic excitations will be introduced and discussed. The periodic excitation with cycle time τ may be represented by a periodic triangular function,

$$F_{x,\text{exc}}(t) = A_{\text{exc}}\, f_{\text{tri}}(t) \tag{7}$$

and

$$\begin{aligned} f_{\text{tri}}(t) =& (2 \cdot \left(1 - (\frac{2}{\tau}t - \frac{1}{2}) \bmod 2\right) \\ & \cdot \operatorname{sign}\left(1 - (\frac{2}{\tau}t - \frac{1}{2}) \bmod 2\right) - 1) \end{aligned} \tag{8}$$

with additional excitation force A_{exc}, Figure 4(a) in the box top left. A sinusoidal function may also be considered for investigation,

$$F_{x,\text{exc}}(t) = A_{\text{exc}} \sin\left(\frac{2\pi}{\tau}t\right) \tag{9}$$

with the same level of maximum force excitation as in (7). A corresponding time history of $F_{x,\text{exc}}$ is plotted in Figure 4(b) in the box top left. Periodic ramps, consisting of six segments of length $\tau/6$,

$$F_{x,\text{exc}}(t) = A_{\text{exc}} \min\left(\max\left(1.5 \cdot f_{\text{tri}}(t), -1\right), 1\right) \tag{10}$$

are depicted in the time history of in Figure 4(c) in the box top left. Finally, alternating step excitation,

$$F_{x,\text{exc}}(t) = A_{\text{exc}} \cdot \operatorname{sign}\left((\frac{2}{\tau}t) \bmod 2 - 1\right) \tag{11}$$

are considered and plotted in Figure 4(d) in the box top left.

Accumulated data points from active force excitation (over one cycle) are plotted in Figure 4 to gain some

understanding of their potential effectiveness and to identify potential drawbacks. Nominal values of the differential traction coefficient $\mu_{\Delta,F}$, the front axle slip $s_{x,F}$ and the front differential slip $s_{s,\Delta,F}$ are plotted in magenta color, which result from a vehicle with drive force distribution $\nu = 0.6$ accelerating at 1 m/s^2 on dry asphalt surface. Considering Figure 3(a), it becomes obvious that active excitation forces are essential at the considered drive force distribution (that may be desired from a vehicle handling and stability point of view) to estimate the normalized slip slope $\overline{C}_{s_x,i}$ based on (12).

Obviously, large levels of excitation forces and corresponding differential slips $s_{x,\Delta,i}$ are beneficial to efficiently estimate the normalized slip slope $\overline{C}_{s_x,i}$, see also Figure 3. However, traction coefficient utilization has to be limited to avoid critical conditions while running on (yet unknown) low friction potential road surfaces. Moreover, periods of keeping a constant velocity (or acceleration), e.g. driving on highways, may lead to packed data points and may reduce estimation quality.[21] Periodic excitations may help to prevent such conditions.

Superimposing similar levels of active excitation to the drive force demanded by the human/robot driver, an equal distribution of data points is present at periodic triangular excitation functions, Figure 4(a). This persistent excitation may be beneficial from an estimator point of view. Moreover, this continuous pattern may be easily realized in vehicle application. Sinusoidal excitation results in slightly accumulated data points in levels of higher differential slips, Figure 4(b), that might be in favor for fast detection of slip slope changes. Since it is smooth, it might be in favour considering the driver's subjective perception of the excitation. Accumulated data points resulting from periodic ramps, Figure 4(c), may result in similar figures as for sinusoidal excitations. However, in contrast to the latter, periods of high levels of excitations may be modified more easily. The alternating steps, Figure 4(d), are considered to be most effective w.r.t. fast detection since the sudden change to the full excitation amplitude immediately generates large differential slip. Therefore the potential estimation errors also gets large immediately, enabling the CUSUM change detection,[23] to reach its threshold quickly.

Considering nominal values of $F_{x,\text{sum}}$ (and thus nominal slip $s_{x,F}$, magenta dots in Figure 4) close to zero, e.g. driving at constant and rather low velocity, sufficient (periodic) excitation levels may result in (small) negative drive forces $F_{x,i}$ that can be realized by recuperation.

Parameter estimation

Since the system (6) is nonlinear in the parameters $\overline{C}_{s_x,i}$ and λ, e.g. an extended Kalman filter[24] is set up. Depending on the formulation of (6), the slip stiffness ratio λ appears in the nominator or denominator of the scaling term of $\mu_{\Delta,i}$. Thus, in the Kalman filter output equation λ or $1/\lambda$, respectively, is substituted by β,

$$\begin{aligned} y_k &= h_k(\underline{x}_k, v_k) \\ &= \left(\mu_{i,k} - \beta_i \frac{r_{e,j}\,\omega_{j,k}}{r_{e,i}\,\omega_{i,k}}\mu_{j,k}\right) \frac{1}{\overline{C}_{s_{x,i,k}}} + \overline{\delta}_{i,k} + v_k \quad (12) \\ & i = F, R,\ \ j = R, F, \end{aligned}$$

$$\beta_F = \frac{1}{\lambda} \quad \text{and} \quad \beta_R = \lambda \tag{13}$$

with measurement noise v_k. Therefore, the parameter vector to be estimated reads

$$\underline{x}_k = \begin{bmatrix} \frac{1}{\overline{C}_{s_x i\,k}} \\ \beta_{i,k} \\ \overline{\delta}_{i\,k} \end{bmatrix} \qquad i = F, R,\ \ j = R, F, \tag{14}$$

and the model equation of the estimator becomes

$$\underline{x}_k = f_k(\underline{x}_{k-1}, \underline{w}_{k-1}) = \underline{x}_{k-1} + \underline{w}_{k-1} \tag{15}$$

with process noise $\underline{w}_{k-1}$. The parametrization of an extended Kalman filter with constant covariance of the measurement noise $\mathbf{R}$ and covariance of the process noise $\mathbf{Q}$ is a compromise between 'stable' estimation output and fast response to changes. To combine these requirements, a CUSUM change detection algorithm is used, where the prediction error $\epsilon_k = y_k - h_k(\underline{x}_k, 0)$ is accumulated for positive and negative values[23],

$$\nu_{k,cusum} = \epsilon_k \tag{16}$$

$$\underline{g}_k = \underline{g}_{k-1} + \begin{bmatrix} \nu_{k,cusum} \\ -\nu_{k,cusum} \end{bmatrix} - \underline{\zeta} \tag{17}$$

As $g_{k,n}$ $(n \in 1, 2)$ reaches a selected threshold, the error covariance matrix $\mathbf{P}$ is reset to allow for a fast adaption of $\overline{C}_{s_x}$ and δ.

If the currently estimated normalized differential slip slope $\overline{C}_{s_x,i}$ is higher than the actual slip slope, positive differential slip results in a positive prediction error ϵ, and negative differential slip results in a negative prediction error, Figure 5(a). To overcome this shortcoming, ϵ is multiplied with the sign of the differential slip, Figure 5(a),

$$\nu_{k,cusum} = \text{sgn}(s_{x,\Delta,i,k})\,\epsilon_k \tag{18}$$

A comparison of $g_{k,i}$ between the use of (16) and (18) in (17) is reported in Figure 5(b). It is obvious that with the modified prediction error for both, positive and negative differential slip, $g_{k,2}$ increases as desired. This is not the case applying the original formulation.

Simulation results

To evaluate the impact of the active excitations (7)-(11) on the availability and responsiveness of the estimated normalized slip slope $\overline{C}_{s_x,F}$, these excitations are applied to a basic half-car vehicle model and the Kalman filter presented above. The half-car vehicle model includes vehicle translational motion (19), and the front and rear axle (wheel) dynamics, (20) and (21), $x = [v_x,\ \omega_F,\ \omega_R]^{\mathrm{T}}$,

$$\dot{x}_1 = \frac{1}{m}\left(F_{x,F} + F_{x,R} - C_D\,x_1^2\right) \tag{19}$$

$$\dot{x}_2 = \frac{1}{I_F}\left(M_F(t) - r_{l,F}F_{x,F} - r_{D,F}F_{z,F}\right) \tag{20}$$

$$\dot{x}_3 = \frac{1}{I_R}\left(M_R(t) - r_{l,R}F_{x,R} - r_{D,R}F_{z,R}\right) \tag{21}$$

with the vehicle mass m, wheel inertia for the front and rear axle I_i, drag coefficient $C_D = 0.5\,A\,c_d\,\rho$, the loaded

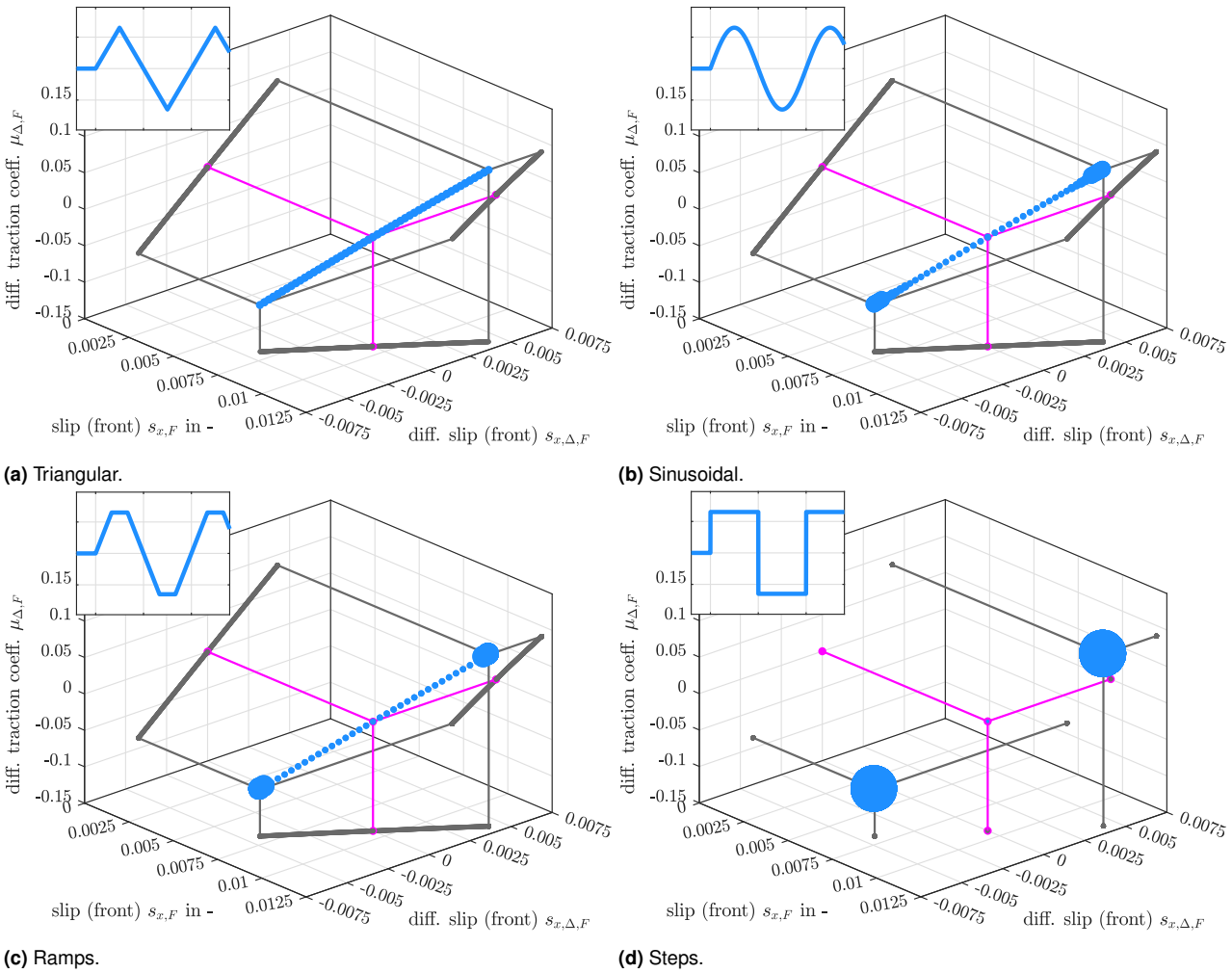

(a) Triangular. **(b)** Sinusoidal. **(c)** Ramps. **(d)** Steps.

Figure 4. Active force excitation accumulated over one period with cycle time τ: differential traction coefficient $\mu_{\Delta,F}$, front axle slip $s_{x,F}$ and front differential slip $s_{x,\Delta,F}$.

wheel radii $r_{l,i}$ and the rolling resistance coefficient $r_{D,i}$. Longitudinal tire forces are calculated applying the pure longitudinal brush tire model[22]. Since driving at constant velocity and at almost constant, low levels of acceleration is considered only, and cycle times of above introduced periodic active drive force excitation are rather long, transient tire behavior and dynamic wheel load transfer are not taken into account in the simulation model. Hence, wheel loads $F_{z,i}$ are assumed to be (quasi) statically dependent on the longitudinal acceleration, (22) and (23),

$$F_{z,F} = F_{z,F0} - \Delta F_z(\dot{x}_1) \tag{22}$$
$$F_{z,R} = F_{z,R0} + \Delta F_z(\dot{x}_1) \tag{23}$$

where

$$\Delta F_z = \frac{m\,h}{l_F + l_R}\,\dot{x}_1 \tag{24}$$

with the height over ground of the center of mass h and its distance to the front and rear axle l_i.

Time histories of the evolution of the estimated normalized slip slope $\overline{C}_{s_x,F}$ without active excitation and for several types of active excitation are plotted in Figure 6, where equal estimator parameters (covariance of the measurement noise $\mathbf{R}$, covariance of the process noise $\mathbf{Q}$, and parameters of CUSUM change detection) are selected. These parameters where chosen applying a heuristic approach based on simulation and measurement data, to guarantee for both fast change detection and robust estimates to avoid misdetections. Vehicle, tire and estimator parameters are given in Table 1.

In Figure 6, it is assumed that the initial normalized slip slope $\overline{C}_{s_x,F}$ corresponds to dry asphalt, where the actual slip slope refers to snowy surface conditions. The cycle time of one period of active excitation is selected $\tau = 8\,\mathrm{s}$ and applied at $t = 0\,\mathrm{s}$, the force amplitude A_{exc} is set to 250 N. Two maneuvers are considered: accelerating the vehicle from standstill with almost constant acceleration of 1 m/s^2 (solid lines), corresponding to the nominal conditions depicted in magenta in Figure 4, and operating the vehicle at the constant velocity $v_x = 28\,\mathrm{m/s}$ (100 kph) (dashed lines).

Obviously, for the given vehicle, tire and drive train configuration with constant drive force distribution $\nu = 0.6$, and the level of tire forces from accelerating or driving at constant velocity, the estimator does almost not respond to changes in the normalized slip slope $\overline{C}_{s_x,F}$ (Figure 6, grey line), in contrast to superimposing periodic excitation forces. In the acceleration case, solid lines in Figure 6, it

Table 1. Vehicle, tire and estimator parameters

Vehicle model parameters			
vehicle mass	m	2600	kg
distance CG - front axle	l_F	1.74	m
distance CG - rear axle	l_R	1.16	m
height CG over ground	h	0.425	m
roll. res. coeff. front	$r_{D,F}$	0.0068	-
roll. res. coeff. rear	$r_{D,R}$	0.0069	-
drive force distribution	ν	0.6	-
drag coefficient	C_D	0.371478	kg/m
tire model parameters			
slip slope F	$\overline{C}_{s_x,F}\ (= 2c_{px,F}a^2 \cdot 2/F_{z,F})$	30 / 10	-
slip slope R	$\overline{C}_{s_x,R}\ (= 2c_{px,R}a^2 \cdot 2/F_{z,R})$	30 / 10	-
max. friction coefficient	$\mu_{\max}$	1 / 0.4	-
Estimator parameters			
meas. noise covariance	$\mathbf{R}$	1	-
process noise covariance	$\mathbf{Q}$	diag[1e−5, 1e−5,1e−10]	-
CUSUM drift parameter	ζ_{pos}, ζ_{neg}	2e−4	-
CUSUM threshold	$th_p\ th_n$	0.2	-
estimator cycle time	T_0	0.02	s

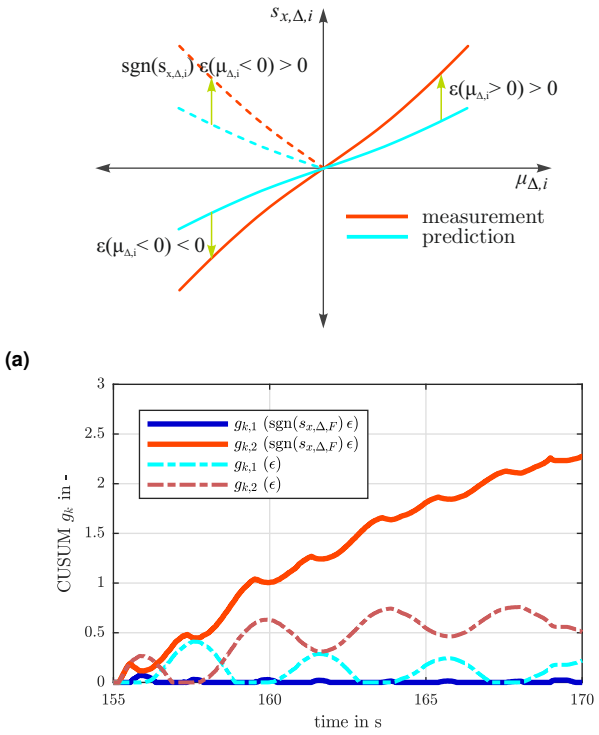

Figure 5. (a) Calculation of $\nu_{k,cusum}$ from prediction error ϵ_k and differential slip $s_{x,\Delta,k}$, and (b) time history of g_k applying (16) and (18)

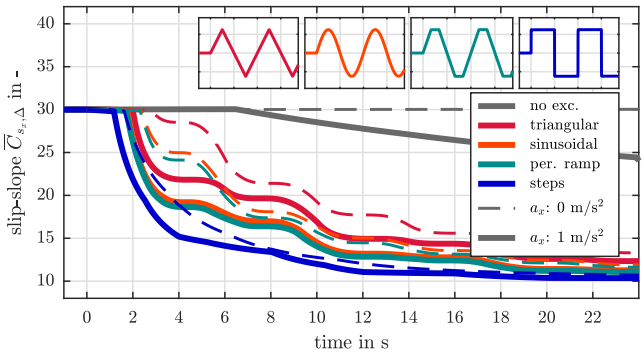

Figure 6. Time history of estimated normalized slip slope $\overline{C}_{s_x,F}$ for different excitation functions and acceleration levels; $F_{x,\text{sum}} = 2600\,\text{N}$ (corresponding to $a_x = 1\,\text{m/s}^2$) and $290\,\text{N}$ (corresponding to $a_x = 0\,\text{m/s}^2$); $A_{\text{exc}} = 250\,\text{N}$ (corresponding to a traction coefficient of $\mu_i = 0.15$ and 0.04, respectively); $\tau = 8\,\text{s}$.

becomes obvious that from periodic triangular, sinusoidal and periodic ramp excitation, the estimator initially responds similar and clearly slower to changes of the normalized slip slope $\overline{C}_{s_x,F}$ than to the periodic step excitation. The rapid response to the latter may be mainly attributed to the early triggering of the CUSUM change detection, accumulating the scaled estimation error of the Kalman filter and adapting respective parameters. Before CUSUM is triggered, very low adaption of the Kalman filter may be noticed from $t = 0\,\text{s}$ to approx. $1.5\,\text{s}$, resulting from its rather slow and robust design in nominal conditions. This behavior also highlights the significance of the tuning of the change detection parameters. Regarding the periodic triangular, step and sinusoidal active excitation it becomes obvious that for the selected nominal drive force distribution $\nu = 0.6$ (see Figure 3) at $t = 4\,\text{s}$, $8\,\text{s}$ and $12\,\text{s}$ no progress in the estimation of the normalized slip slope $\overline{C}_{s_x,F}$ is made. Since this is not the case for the periodic step excitation, the actual value of the normalized slip slope $\overline{C}_{s_x,F} = 10$ is approached earlier.

While driving at constant velocity, the response of the estimator to the individual types of active excitation is similar to the accelerating case. However, in general, changes of the normalized slip slope $\overline{C}_{s_x,F}$ are detected about $0.5\,\text{s}$ later, and the initial drop of $\overline{C}_{s_x,F}$ is considerably reduced compared to the acceleration case. While the initial drop for sinusoidal, periodic ramp and step excitation may be sufficient to indicate possible changes in the road surface

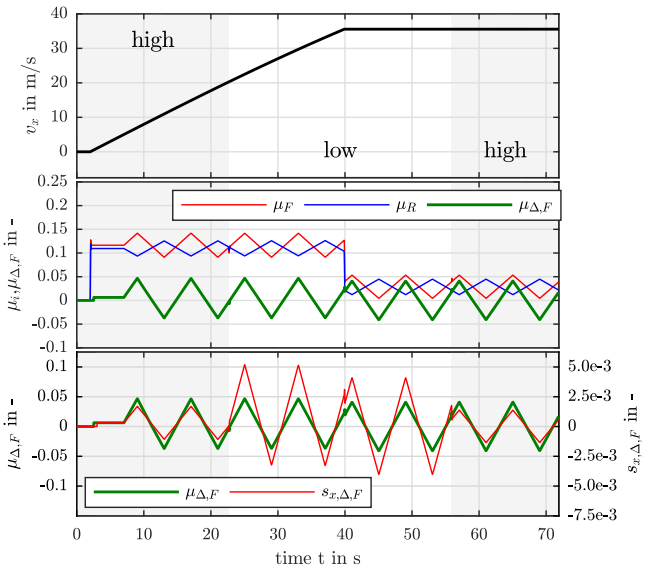

Figure 7. Different acceleration levels and friction potentials: Traction coefficients μ_i, differential traction coefficient $\mu_{\Delta,F}$ and differential slip $s_{x,\Delta,F}$; periodic triangular excitation function; $A_{\text{exc}} = 250\,\text{N}$; $\tau = 8\,\text{s}$.

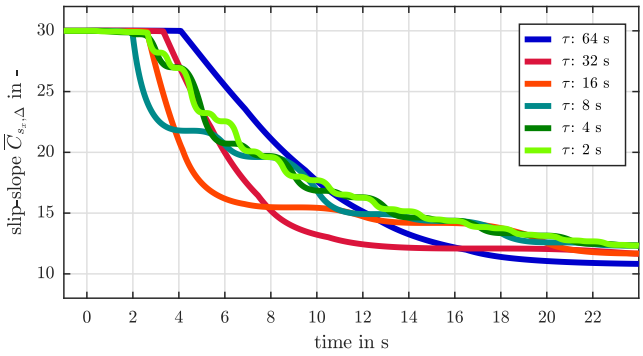

Figure 8. Time history of estimated normalised slip slope $\overline{C}_{s_x,F}$ for different cycle times τ; periodic triangular excitation function; $F_{x,\text{sum}} = 2600\,\text{N}$ (corresponding to $a_x = 1\,\text{m/s}^2$); $A_{\text{exc}} = 250\,\text{N}$.

and thus friction potential changes, for the periodic triangular excitation, a fast detection is unlikely. This is in particular interesting, since the tires are operated in their 'linear' regime at both $a_x = 1\,\text{m/s}^2$ and $a_x = 0\,\text{m/s}^2$.

A related time history of the actual traction coefficients μ_i, the differential traction coefficient $\mu_{\Delta,F}$, and the differential slip $s_{x,\Delta,i}$ is plotted in Figure 7, exemplarily for the periodic triangular excitation. The vehicle is accelerated from standstill with $a_x = 1\,\text{m/s}^2$ until $t = 38\,\text{s}$, where the velocity is kept constant at $v_x = 36\,\text{m/s}$, Figure 7(top). Grey background color represents dry road conditions, while white background color represents snowy road conditions. At $t = 0\,\text{s}$, nominal traction coefficients μ_i correspond to the nominal values depicted in Figure 4. Active excitation is applied after five seconds at a minimum speed of $v_x = 5\,\text{m/s}$. While the mean level of the actual traction coefficients μ_i drops at stopping accelerating the vehicle, Figure 7(center), the differential traction coefficient $\mu_{\Delta,F}$, resulting from the active excitation, is (almost) not affected. However, at approaching the low friction surface at $t = 21\,\text{s}$, the differential slip $s_{x,\Delta,F}$ increases, Figure 7(bottom), resulting from the drop of the normalized slip slope $\overline{C}_{s_x,F}$, until the vehicle re-enters dry road conditions at $t = 54\,\text{s}$. A shift of the differential slip $s_{x,\Delta,F}$ may be noticed at stopping accelerating the vehicle, due to the shift of some wheel load from the rear to the front. Since this shift results in late triggering of the CUSUM change detection, less effective detection of changes in the normalized slip slope may be expected, highlighting again the impact of the tuning of the CUSUM change detection.

Since the friction potential is (considered to be) unknown, freedom on the selection of the active excitation force A_{exc} is very limited (in practical application) to avoid critical driving conditions introduced from excessive friction potential utilization, in particular on low friction surfaces. However, A_{exc} may be adapted to the actual driving conditions, considering the actual (requested) traction coefficient. In the case of driving at constant velocity in Figure 6, the excitation level may be increased at straight driving to $A_{\text{exc}} = 1000\,\text{N}$, corresponding to a maximum traction coefficient $\mu_i \approx 0.1$. In this case, the response to changes in the normalized slip slope is increased significantly, similar to accelerating at $1\,\text{m/s}^2$, however, partial recuperation is needed. In addition, adjusting the CUSUM change detection parameters continuously to the level of active excitation may also increase the efficiency while guaranteeing for robustness of the algorithm.

The significant impact of the cycle time τ of the periodic active excitation on the evolution of the estimated normalized slip slope $\overline{C}_{s_x,F}$ becomes obvious from Figure 8. The vehicle is accelerated at $a_x = 1\,\text{m/s}^2$; except from the cycle time, other parameters correspond to parameters applied for Figure 6. The figure shows a comparison for different cycle times τ from 64 s to 2 s for the periodic triangular active excitation. With decreasing cycle times, the time until a change in the normalized slip slope is detected, decreases, and reaches the minimum for $\tau \approx 8\,\text{s}$. For shorter cycle times, the detection time increases, since the excitation is not sufficient to trigger the CUSUM change detection algorithm.

In practical application, certain constraints limit reasonable types of active excitation, excitation force levels, and frequencies. Besides safe operation, as mentioned above, feasible technical realization and in particular the human (co-) driver's perception of the excitation shall be mentioned.

Besides the types of excitation, the parameters of the estimator have a considerable influence on the change detection behavior. In practical application they have to be selected not only with respect to the detection and adaption time, but also taking the actual noise and expected variation of input signals from disturbances into account. These quantities may vary considerably depending on the actual vehicle (properties) and the implemented sensors. An exemplary comparison of the estimated slip slope with four different process noise covariance matrix entries $Q_{(1,1)}$ (different colors) and three different CUSUM thresholds (line style) is shown in Figure 9. Large entries in the process covariance matrix (dark cyan line) allow fast adaption rates that can be used for detection of rapid changes, but cause the filter to be sensitive to disturbances, which are not considered in this simulation study. In this case the filter adapts to the new levels of slip slope before the CUSUM threshold

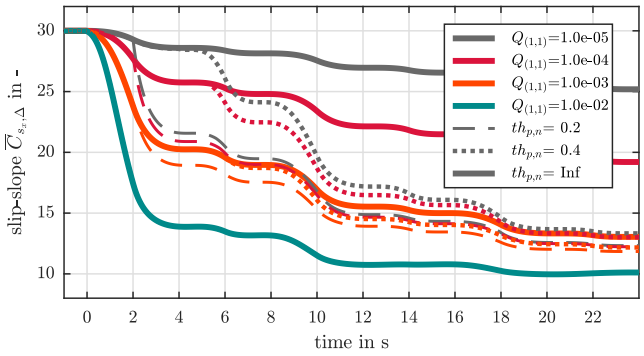

Figure 9. Time history of estimated normalised slip slope $\overline{C}_{s_x,F}$ for different Kalman filter and change detection parameters $Q_{(1,1)}$ and $th_{p,n}$; periodic triangular excitation function; $F_{x,\text{sum}} = 2600\,\text{N}$ (corresponding to $a_x = 1\,\text{m/s}^2$); $A_{\text{exc}} = 250\,\text{N}$.

is reached. With smaller $Q_{(1,1)}$ entries, the adaption rates decrease and the change detection is beneficial to increase detection and adaption time.

Experimental results

To assess the effectiveness of the proposed approach and the subjective perception of the active excitation, the amplitude A_{exc} and the cycle time τ was varied at test drives utilizing an electric all-wheel drive car with one motor on each axle. For straight forward implementation to the modified drive force distribution controller, the sinusoidal active excitation (9) was applied. Main parameters of the test vehicle are similar to parameters given in Table 1. Measurements on low friction surfaces were performed on closed tracks on an frozen lake with rough ice covered with a thin snow layer. High friction surface maneuvers were recorded on the same day, with the same car and tires, on public roads near the test track on dry asphalt.

In Figure 10, measurements on dry asphalt (gray) and snow surface (white) with nominal drive force distribution $\nu = 0.5$, and with excitation amplitude $A_{\text{exc}} = 0.2\,F_{x,\text{sum}}$ and cycle time $\tau = 8\,\text{s}$ are combined and reported. A sequence of four acceleration (and deceleration) maneuvers ($a_x \approx 2\,\text{m/s}^2$) up to $v_x = 22\,\text{m/s}$ is conducted, Figure 10(top), where the estimator is activated during acceleration only. The nominal drive force distribution was set until $t = 65\,\text{s}$, followed by activated drive force excitation. It is obvious that the differential traction coefficient $\mu_{\Delta,F}$ is considerably increased with active drive force excitation, Figure 10(center top), while the overall level of traction coefficient utilization (μ_i) remains similar to the nominal case. Hence, the changed differential slip $s_{x,\Delta,F}$ results in successful and rather fast detection of changes of the normalized slip slope $\overline{C}_{s_x,F}$ due to both increasing and decreasing friction potential, Figure 10(center bottom, bottom), which is not the case with nominal drive force distribution.

From a subjective perception point of view, at driving on a straight, the skilled (co-)driver reported that cycle times below $4\,\text{s}$ have been audible only, while changed vehicle behavior has not been perceived.

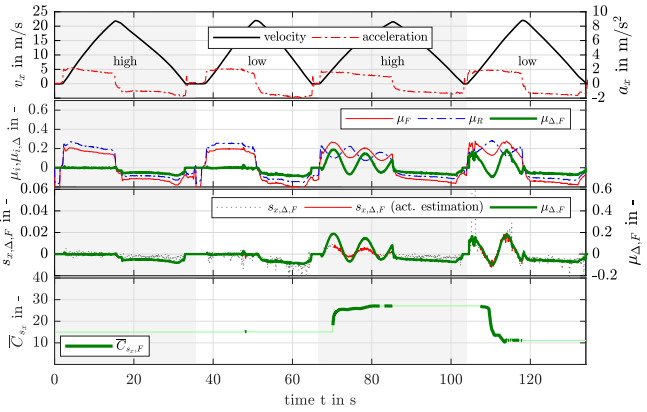

Figure 10. Field tests – acceleration (and deceleration) maneuvers on dry asphalt and snow surface with fixed force distribution $\nu \approx 0.5$ and an active sinusoidal force excitation: longitudinal velocity v_x and acceleration a_x, traction coefficients μ_i and differential traction coefficient $\mu_{\Delta,F}$, differential traction coefficient $\mu_{\Delta,F}$ and differential slip $s_{x,\Delta,F}$, estimated normalized slip slope $\overline{C}_{s_x,F}$; $A_{\text{exc}} = 0.2\,F_{x,\text{sum}}$ ($\approx 500\,\text{N}$); $\tau = 8\,\text{s}$.

Conclusions

The proposed method allows to estimate slip slope (changes) with the knowledge of the wheel speed and tire radii ratio between front and rear tires – that may be estimated during constant drive or coasting maneuvers –, vertical tire loads and drive forces only. The method is further applicable to all-wheel drive vehicles with mixed tires. In particular, active drive force excitation may improve availability of the estimates considerably. Different periodic excitation shape functions have been investigated w.r.t. the need for persistent excitation and responsiveness of the estimator, but also considering drive force excitation levels and cycle times, bearing in mind both vehicle safety and passengers comfort.

Vehicle tests with a passenger car showed that even very small superimposed drive force amplitudes (additional traction force coefficient utilization smaller than 0.05) allows for sufficient change of the differential slip and traction coefficient, leading to very high availability and sensitivity of the estimates. Moreover, tests have shown that effective drive force amplitudes and cycle times are not recognized by the (co-)driver at straight ahead driving.

Acknowledgements

The authors thank Florian Büttner for conducting the field measurements.

References

1. Müller S, Uchanski M and Hedrick K. Estimation of the maximum tire-road friction coefficient. *Journal of Dynamic Systems, Measurement, and Control* 2004; 125(4): 607–617. DOI:10.1115/1.1636773.
2. RoadCloud. https://roadcloud.com/ accessed 10. 2022; .
3. Andersson M, Bruzelius F, Casselgren J et al. Road friction estimation, part ii. Report, IVSS Project Report, 2010.
4. Svendenius J. *Tire modeling and friction estimation*. Thesis, Lund University, Sweden, 2007.
5. Albinsson A, Bruzelius F, Jacobson B et al. Design of tyre force excitation for tyre-road friction estimation. *Vehicle System*

Dynamics 2017; 55(2): 208–230. DOI:10.1080/00423114.2016.1251598.

6. Lajewski T, Rauh J and Müller S. Single wheel braking-a new method to measure friction potential on public roads. In *The IAVSD International Symposium on Dynamics of Vehicles on Roads and Tracks*. Springer, pp. 1033–1041.
7. Albinsson A, Bruzelius F, Jacobson B et al. Identification of tyre characteristics using active force excitation. In Rosenberger M (ed.) *Dynamics of vehicles on roads and on tracks*. p. 10.
8. Standard test method for determining longitudinal peak braking coefficient of paved surfaces using standard reference test tire. Technical report, International, ASTM, 2002. ASTM Standard E1337-90.
9. Dieckmann T. *Der Reifenschlupf als Indikator für das Kraftschlußpotential*. Thesis, Universität Hannover, 1992.
10. Gustafsson F. Estimation and change detection of tire-road friction using the wheel slip. In *Computer-Aided Control System Design, 1996., Proceedings of the 1996 IEEE International Symposium on*. pp. 99–104. DOI:10.1109/CACSD.1996.555237.
11. Gustafsson F. Slip-based tire-road friction estimation. *Automatica* 1997; 33(6): 1087–1099. DOI:http://dx.doi.org/10.1016/S0005-1098(97)00003-4.
12. Deur J, Ivanović V, Pavković D et al. On low-slip tire friction behavior and modeling for different road conditions. In *CD Proceedings of 19th IAVSD Symposium-Poster Papers*. pp. 1–10.
13. Carlson CR and Gerdes JC. Consistent nonlinear estimation of longitudinal tire stiffness and effective radius. *IEEE Transactions on Control Systems Technology* 2005; 13(6): 1010–1020. DOI:10.1109/TCST.2005.857408.
14. Pavkovic D, Deur J, Asgari J et al. Experimental analysis of potentials for tire friction estimation in low-slip operating mode. *SAE Technical Paper 2006-01-0556* 2006; DOI:10.4271/2006-01-0556.
15. Ahn CS, Peng H and Tseng HE. Robust estimation of road friction coefficient. In *American Control Conference (ACC), 2011*. ISBN 0743-1619, pp. 3948–3953. DOI:10.1109/ACC.2011.5991256.
16. Fichtinger A, Edelmann J, Plöchl M et al. Aquaplaning detection using effect-based methods: An approach based on a minimal set of sensors, electronic stability control, and drive torques. *IEEE Vehicular Technology Magazine* 2021; 16(3): 20–28. DOI:10.1109/MVT.2021.3085536.
17. Miller SL, Youngberg B, Millie A et al. Calculating longitudinal wheel slip and tire parameters using gps velocity. In *Proceedings of the 2001 American Control Conference. (Cat. No.01CH37148)*, volume 3. ISBN 0743-1619, pp. 1800–1805 vol.3. DOI:10.1109/ACC.2001.945995.
18. Klomp M, Gao Y and Bruzelius F. Longitudinal velocity and road slope estimation in hybrid electric vehicles employing early detection of excessive wheel slip. *Vehicle System Dynamics* 2014; 52(Supp. 1): 172–188. DOI:10.1080/00423114.2014.887737.
19. Forssell U, Gustafsson F and Stenman A. Road friction indicator for all wheel drive road vehicles, 2005. Patent EP1558456.
20. Acosta M, Kanarachos S and Blundell M. Road friction virtual sensing: A review of estimation techniques with emphasis on low excitation approaches. *Applied Sciences* 2017; 7(12). DOI:10.3390/app7121230.
21. Stenlund B and Gustafsson F. Avoiding windup in recursive parameter estimation. *Preprints of reglermöte 2002, Linköping, Sweden* 2002; : 148–153.
22. Pacejka HB. *Tire and vehicle dynamics*. Oxford, UK: Butterworth-Heinemann, 2012.
23. Gustafsson F. *Adaptive filtering and change detection*. John Wiley & Sons Ltd, 2000.
24. Simon D. *Optimal State Estimation: Kalman, H infinity, and Nonlinear Approaches*. Hoboken, New Jersey, USA: John Wiley & Sons, Inc., 2006. ISBN 0470045337.